

# Generalized Description of the Spatio-Temporal Biphoton State in Spontaneous Parametric Down-Conversion

Baghdasar Baghdasaryan,<sup>1, 2, \*</sup> Carlos Sevilla,<sup>3</sup> Fabian Steinlechner,<sup>3, 4, †</sup> and Stephan Fritzsche<sup>1, 2, 4</sup>

<sup>1</sup> *Theoretisch-Physikalisches Institut, Friedrich Schiller University Jena, 07743 Jena, Germany*

<sup>2</sup> *Helmholtz-Institut Jena, 07743 Jena, Germany*

<sup>3</sup> *Fraunhofer Institute for Applied Optics and Precision Engineering IOF, 07745 Jena, Germany*

<sup>4</sup> *Abbe Center of Photonics, Friedrich Schiller University Jena, 07745 Jena, Germany*

(Dated: August 23, 2022)

Spontaneous parametric down-conversion (SPDC) is a widely used source for photonic entanglement. Years of focused research have led to a solid understanding of the process, but a cohesive analytical description of the paraxial biphoton state has yet to be achieved. We derive a general expression for the spatio-temporal biphoton state that applies universally across common experimental settings and correctly describes the non-separability of spatial and spectral modes. We formulate a criterion on how to decrease the coupling of the spatial from the spectral degree of freedom by taking into account the Gouy phase of interacting beams. This work provides new insights into the role of the Gouy phase in SPDC, and also into the preparation of engineered entangled states for multidimensional quantum information processing.

Photon pairs generated via spontaneous parametric down-conversion (SPDC) have provided an experimental platform for fundamental quantum science [1] and figure prominently in applications in quantum information processing, including recent milestone experiments in photonic quantum computing [2].

Several works in recent years have addressed the challenge of tailoring the spectral and spatial properties of *signal* and *idler* photons generated via SPDC in theory and experiment. In the spatial domain, that is, the transverse momentum space, much of this work was motivated by the objective of improving fiber coupling efficiency [3, 4] or the dimensionality of spatial entanglement [5–7]. In the spectral domain, the motivation was usually to engineer pure spectral states, which are crucial for protocols based on multiphoton interference [8]. This has been performed either by tailoring the nonlinearity of the crystal [9], by tuning the pump spatial intensity and phase, or by using counter-propagating photon pair generation in periodically poled waveguides [10].

Closed expressions for the state emitted by SPDC in bulk crystals have been derived using very special techniques and approximations, such as the narrowband [11], thin-crystal [12, 13] or plane wave approximations [14], where either the spectral or spatial biphoton state is considered. However, from the *X*-shaped spatio-temporal correlations [15], the spatial and spectral properties of SPDC have been known to be coupled due to the phase matching characteristics. To date, models that address both spectrum and space together have been limited to approximate phase matching functions [16] or numerical calculations [17].

Here, we present a simple-to-use closed expression for the biphoton state. The approach describes the full spectral and spatial properties of all interacting beams and

applies to a wide range of experimental settings. The analytical treatment of the biphoton state decomposed into discrete LG modes will also provide a deeper insight into the role of the Guoy phase in PDC. Next to providing an intuitive understanding, we also demonstrate the utility of the expression for quantum state engineering in multidimensional quantum information processing.

Let us start with the basic expressions of SPDC. Since typical optical apparatuses support only paraxial rays about a central axis, we can make use of the paraxial approximation, where the longitudinal and transverse components of the wave vector can be treated separately  $\mathbf{k} = \mathbf{q} + k^z(\omega) \mathbf{z}$ . Consequently, the biphoton state in the momentum space can be represented by the following expression [18–20]

$$|\Psi\rangle = \iint d\mathbf{q}_s d\mathbf{q}_i d\omega_s d\omega_i \Phi(\mathbf{q}_s, \mathbf{q}_i, \omega_s, \omega_i) \hat{a}_s^\dagger(\mathbf{q}_s, \omega_s) \hat{a}_i^\dagger(\mathbf{q}_i, \omega_i) |vac\rangle. \quad (1)$$

Eq. (1) refers to the generation of photon pairs with energies  $\omega_{s,i}$  and transverse momenta  $\mathbf{q}_{s,i}$  from the vacuum state  $|vac\rangle$ . The biphoton mode function  $\Phi(\mathbf{q}_s, \mathbf{q}_i, \omega_s, \omega_i)$  contains the rich high-dimensional spatio-temporal structure of SPDC that arises from the coupling between the wave vectors of the pump, signal, and idler beams.

The transverse spatial degree of freedom (DOF) has been successfully used in continuous variable information processing [19, 21]. However, in practical experimental settings, the continuous variable space is more often discretized using a set of modes. The proper choice of a set reduces the number of dimensions needed to describe the state. Moreover, discrete modes are easy to manipulate and detect using efficient experimental techniques [22, 23]. Since the projection of the orbital angular momentum (OAM) is conserved in SPDC [24], it is convenient to decompose the biphoton state into LG modes  $|p, \ell, \omega\rangle = \int d\mathbf{q} LG_p^\ell(\mathbf{q}) \hat{a}^\dagger(\mathbf{q}, \omega) |vac\rangle$ , which are

\* [baghdasar.baghdasaryan@uni-jena.de](mailto:baghdasar.baghdasaryan@uni-jena.de)

† [fabian.steinlechner@uni-jena.de](mailto:fabian.steinlechner@uni-jena.de)

eigenstates of OAM [25]:

$$|\Psi\rangle = \iint d\omega_s d\omega_i$$

$$\sum_{p_s, p_i=0}^{\infty} \sum_{\ell_s, \ell_i=-\infty}^{\infty} C_{p_s, p_i}^{\ell_s, \ell_i} |p_s, \ell_s, \omega_s\rangle |p_i, \ell_i, \omega_i\rangle, \quad (2)$$

where the coincidence amplitudes are calculated from the overlap integral  $C_{p_s, p_i}^{\ell_s, \ell_i} = \langle p_s, \ell_s, \omega_s; p_i, \ell_i, \omega_i | \Psi \rangle$ ,

$$C_{p_s, p_i}^{\ell_s, \ell_i} = \iint d\mathbf{q}_s d\mathbf{q}_i \Phi(\mathbf{q}_s, \mathbf{q}_i, \omega_s, \omega_i) [\text{LG}_{p_s}^{\ell_s}(\mathbf{q}_s)]^*$$

$$\times [\text{LG}_{p_i}^{\ell_i}(\mathbf{q}_i)]^*. \quad (3)$$

The summations in Eq. (2) run over the LG mode numbers  $p$  and  $\ell$  associated with the radial momentum and the OAM projection, respectively. Except for the fact, that we now deal with summations instead of integrations, this discretization will also help us to understand the coupling of spatial and spectral DOF in the frame of the Gouy phase of LG modes.

The construction of the biphoton state reduces to the calculation of the coincidence amplitudes  $C_{p_s, p_i}^{\ell_s, \ell_i}$ , which in turn depend on the mode function  $\Phi(\mathbf{q}_s, \mathbf{q}_i, \omega_s, \omega_i)$ . A compact expression for the mode function can be derived if the experimental setup is fixed.

Here, we consider the scenario when a coherent laser beam propagates along the  $z$ -axis and is focused in the middle of a nonlinear crystal placed at  $z = 0$ . Signal and idler fields propagate close to the pump direction, known as the quasi-collinear regime. The crystal and the pump beam have typical transverse cross sections in the order of  $mm$  and  $\mu m$ , respectively. Hence, we assume that the crystal compared to the pump beam is infinitely extended in the transverse direction, which enforces the conservation of the transverse momentum,  $\mathbf{q}_p = \mathbf{q}_s + \mathbf{q}_i$  [18]. Taking into account also the energy conservation  $\omega_p = \omega_s + \omega_i$ , the mode function can be written as [20]

$$\Phi(\mathbf{q}_s, \mathbf{q}_i, \omega_s, \omega_i) = N_0 V_p(\mathbf{q}_s + \mathbf{q}_i) S_p(\omega_s + \omega_i)$$

$$\times \int_{L/2}^{-L/2} dz \exp \left[ i(k_p^z - k_s^z - k_i^z)z \right], \quad (4)$$

where  $N_0$  is the normalization constant,  $V_p(\mathbf{q}_p)$  is the spatial, and  $S_p(\omega_p)$  is the spectral distribution of the pump beam, and  $L$  is the length of the nonlinear crystal along  $z$ -axis.

The important component of the mode function (4) is the phase mismatch in the  $z$ -direction  $\Delta k^z = k_p^z - k_s^z - k_i^z$ , which characterizes the differences in the energies and momenta of the signal and idler photons. Therefore, careful calculation of  $\Delta k^z$  is essential for the quantitative description of SPDC, which we will do next.

Experimentally generated lights are usually not monochromatic and contain a frequency distribution. Therefore, except for the central frequencies that meet

energy conservation condition  $\omega_p^0 = \omega_s^0 + \omega_i^0$ , we expect a deviation from them,  $\omega = \omega^0 + \Omega$  with the assumption  $\Omega \ll \omega^0$ . Furthermore, in the paraxial approximation, the transverse component of the momentum is much smaller than the longitudinal component  $|\mathbf{q}| \ll k$ . With this in mind, we can apply the Taylor series on  $k^z$  (Fresnel approximation) to  $|\mathbf{q}|/k$  and also to small  $\Omega$ :

$$k^z = k(\Omega) \sqrt{1 - \frac{|\mathbf{q}|^2}{k(\Omega)^2}} \approx k + \frac{\Omega}{u} + \frac{G\Omega^2}{2} - \frac{|\mathbf{q}|^2}{2k},$$

where  $u = 1/(\partial k/\partial \Omega)$  is the group velocity and  $G = \partial/\partial \Omega (1/u)$  is the group velocity dispersion, evaluated at the respective central frequency. Here, we also assume that the propagation is along a principal axis of the crystal, so we can ignore the Poynting vector walk-off of extraordinary beams in the crystal. Next, we insert the corresponding  $k^z$  of the signal, idler, and pump into the phase mismatch  $\Delta k^z = k_p^z - k_s^z - k_i^z$  and arrive at

$$\Delta k^z = \Delta_\Omega + \rho_s^2 \frac{k_p - k_s}{2k_p k_s} + \rho_i^2 \frac{k_p - k_i}{2k_p k_i} - \frac{\rho_s \rho_i}{k_p} \cos(\varphi_i - \varphi_s) \quad (5)$$

where the frequency part  $\Delta_\Omega$  is given by

$$\Delta_\Omega = \frac{\Omega_s + \Omega_i}{u_p} - \frac{\Omega_s}{u_s} - \frac{\Omega_i}{u_i} + \frac{G_p(\Omega_s + \Omega_i)^2}{2}$$

$$- \frac{G_s \Omega_s^2}{2} - \frac{G_i \Omega_i^2}{2}. \quad (6)$$

In Eq. (5), we used cylindrical coordinates  $\mathbf{q} = (\rho, \varphi)$  with  $\rho_p^2 = \rho_s^2 + \rho_i^2 + 2\rho_s \rho_i \cos(\varphi_i - \varphi_s)$  and assumed momentum conservation for central frequencies  $\Delta k = k_p - k_s - k_i = 0$ . The condition  $\Delta k = 0$  ensures constructive interference in the crystal between the pump, signal, and idler beams, which is usually performed with birefringent crystals [20] or more recently by periodic poling along the crystal axis,  $k_p - k_s - k_i - 2\pi/\Lambda = 0$ , where  $\Lambda$  is the poling period [26].

The remaining components of the mode function (4) that we should still fix are the pump characteristics. We model the angular distribution with a LG beam. The advantage of this choice is that an arbitrary paraxial optical field can be expressed as a sum of LG beams  $\sum_n a_n \text{LG}_{p_n}^{\ell_n}$  with  $\sum_n |a_n|^2 = 1$  by using their completeness relation. Thus, the theory developed for the LG pump can be easily extended to SPDC with a particular pump. The amplitudes (7) can then be upgraded to revised amplitudes  $\sum_n a_n C_n$ , which follows from Eq. (3). Finally, the temporal distribution is modeled with a Gaussian envelope of pulse duration  $t_0$ ,  $S_p(\omega_p) = \exp(-\omega_p^2 t_0^2/4) t_0/\sqrt{\pi}$  [27], but which can be extended to any arbitrary pump spectrum.

We can now calculate the coincidence amplitudes  $C_{p_s, p_i}^{\ell_s, \ell_i}$  using Eqs. (3)-(6). The following steps are technical and do not include any physical interpretation. Therefore, we summarized them briefly in the supplementary. The final expression for the coincidence amplitudes

for  $\ell \geq 0$  reads

$$\begin{aligned}
C_{p,p_s,p_i}^{\ell,\ell_s,\ell_i} = & N_0 \pi^{3/2} t_0 e^{-\frac{t_0^2(\Omega_s+\Omega_i)^2}{4}} \delta_{\ell,\ell_s+\ell_i} \\
& \sum_{u=0}^p \sum_{s=0}^{p_s} \sum_{i=0}^{p_i} T_u^{p,\ell} (T_s^{p_s,\ell_s})^* (T_i^{p_i,\ell_i})^* \sum_{n=0}^{\ell} \sum_{m=0}^u \\
& \binom{\ell}{n} \binom{u}{m} \sum_{f=0}^{u-m} \sum_{v=0}^m \binom{u-m}{f} \binom{m}{v} \Gamma[h] \Gamma[b] \\
& \int_{-L/2}^{L/2} dz e^{iz\Delta_\Omega} \frac{D^d}{H^h B^b} {}_2\tilde{F}_1 \left[ h, b, 1+d, \frac{D^2}{H B} \right]
\end{aligned} \tag{7}$$

and  $C_{p,p_s,p_i}^{\ell,\ell_s,\ell_i} = (C_{p,p_s,p_i}^{-\ell,-\ell_s,-\ell_i})^*$  for  $\ell \leq 0$ , where we used a new notation for  $C_{p,p_i}^{\ell,\ell_i}$  to emphasize the mode numbers of the LG pump  $p$  and  $\ell$ . The function  ${}_2\tilde{F}_1$  is known as the *regularized hypergeometric* function [28]. The missing coefficients of Eq. (7) are given by

$$\begin{aligned}
H &= \frac{w_p^2}{4} + \frac{w_s^2}{4} - iz \frac{k_p - k_s}{2k_p k_s}, & D &= -\frac{w_p^2}{4} - iz \frac{1}{2k_p}, \\
B &= \frac{w_p^2}{4} + \frac{w_i^2}{4} - iz \frac{k_p - k_i}{2k_p k_i}, & d &= \ell_i + m - n - 2v, \\
h &= \frac{1}{2}(2 + 2s + \ell + \ell_i + 2(-f + u) - 2n - 2v + |\ell_s|), \\
b &= \frac{1}{2}(2 + 2f + 2i + \ell_i + 2m - 2v + |\ell_i|), \\
T_u^{p,\ell} &= \sqrt{\frac{p! (p+|\ell|)!}{\pi}} \left( \frac{w}{\sqrt{2}} \right)^{2u+|\ell|+1} \frac{(-1)^{p+u} (i)^\ell}{(p-u)! (|\ell|+u)! u!}
\end{aligned}$$

where  $w_p$ ,  $w_s$  and  $w_i$  are the beam waists of the pump, signal and the idler beams, respectively.

The analytical expression (7) for the mode amplitudes as a function of the pump mode constitutes the main result of this work. It allows the spatial and spectral emission profiles to be reconstructed mode by mode and is applicable in any experimental setting that exhibits cylindrical symmetry. It can be readily used to calculate many characteristics of SPDC: joint spectral density, photon bandwidths, pair-collection probability, heralding ratio, spectral and spatial entanglement, etc. Previously, these could only be achieved through numerical calculations or for special cases with a limited scope of applicability. Note that the experimental demonstration of Eq. (7) will be presented in a follow-up paper, where we will show how the coupling of spatial and spectral DOF deteriorates the spatial entanglement but can be compensated directly by a proper choice of the collection mode.

The spatio-temporal coupling encoded in Eq. (7) is a fundamental feature of SPDC. However, the usual applications in quantum optics utilize either the spatial or spectral DOF, neglecting the correlation between them. Nevertheless, this coupling remains a fundamental issue in many protocols based on entangled photon sources,

where any distinguishability arising from not-considered DOF reduces the coherence of the state. Next, we will illustrate the utility of the analytical expression (7) in the frame of possible decoupling of spatial and spectral DOF  $\Phi(\mathbf{q}_s, \mathbf{q}_i, \omega_s, \omega_i) = \Phi_{\mathbf{q}}(\mathbf{q}_s, \mathbf{q}_i) \Phi_{\omega}(\omega_s, \omega_i)$ . We will show that this decoupling is closely related to the Gouy phase of interacting beams.

The role of the Gouy phase in nonlinear processes has been investigated before. For instance, in SPDC, the change of the Gouy phase  $\psi_G(z) = (N+1) \arctan(z/z_R)$  within the propagation distance has been used to control the relative phase of two different LG modes of measurement basis [29, 30]. Here,  $N$  is the combined LG mode number  $N = 2p+|\ell|$  and  $z_R$  is the Rayleigh length  $z_R = n\pi w^2/\lambda$ . In four-wave mixing (FWM), the conversion behavior between LG modes is strongly affected by the Gouy phase [31]. The authors observed that the existence of a relative Gouy phase between modes with different mode numbers  $N$  leads to a reduced FWM efficiency.

Here, we have a similar situation: pump, signal, and idler fields acquire different Gouy phases along with propagation in the crystal due to different mode numbers  $N$ , causing a reduced efficiency of mode down-conversion. We expect intuitively that the shape of the spectrum of spatial modes is affected by the relative Gouy phase of interacting beams. This is still a guess and requires proof.

We consider for simplicity the scenario in which the Rayleigh lengths of the three beams are equal  $z_{R,p} = z_{R,i} = z_{R,s}$  and fixed. This condition matches the Gouy angle  $\arctan(z/z_R)$  for all beams. Hence, the relative Gouy phase can be written as

$$\psi_{G,p} - \psi_{G,s} - \psi_{G,i} = (N_p - N_s - N_i - 1) \arctan(z/z_R),$$

which implies that it is fully defined by the relative mode number  $N_R = N_p - N_s - N_i$ . If the Gouy phase is responsible for different spectral dependencies of the coincidence amplitudes  $C_{p,p_s,p_i}^{\ell,\ell_s,\ell_i}(\Omega_s, \Omega_i)$ , the shape of the spectrum should remain the same for fixed  $N_R$ . Assuming  $k_p \approx 2k_s$ , Eq. (7) transforms into

$$C_{p,p_s,p_i}^{\ell,\ell_s,\ell_i}(\Omega_s, \Omega_i) \propto \int_{-L/2}^{L/2} dz e^{iz\Delta_\Omega} \frac{(i2z + k_p w_p^2)^{N_R}}{(-i2z + k_p w_p^2)^{N_R+1}}. \tag{8}$$

This proves our guess that the spectral dependence of the coincidence amplitudes remains unaffected up to a constant if  $N_R$  is fixed or, i.e., if the relative Gouy phase is unchanged.

This proof brings us a step forward in the decoupling problem of spatial and spectral DOF: the decoupling can be achieved for a selected subspace of modes that possess the same relative Gouy phase. So, if a state is engineered that consists of modes with  $N_R = \text{const.}$ , then the modes contributing to the state have the same spectrum, i.e., the state is separable. The question of decoupling of spatial and spectral DOF can be now reformulated: How

do we engineer a state consisting of modes with the same relative mode number  $N_R$ .

The state engineering in spatial DOF has been investigated theoretically in the thin crystal regime [32, 33] and also implemented experimentally [34, 35], but by neglecting the spectral DOF. In particular, in Ref. [34], three, four, five,-dimensional entangled states in OAM basis have been engineered by using a simultaneous perturbation stochastic approximation algorithm [36]. We have shown in the supplementary that the same states can be constructed in a more straightforward way by using Eq. (7), where no optimization algorithm is needed.

For illustration, we consider a similar four-dimensional state in OAM basis, compare its engineering efficiency with the state from Ref. [34] and investigate on it the spatio-temporal coupling. We use for all our calculations the same experimental parameters as in Ref. [34]: 15-mm-thick periodically poled KTiOPO<sub>4</sub> crystal designed for a collinear frequency degenerate type-II phase matching, continuous-wave laser of wavelength 405 nm with beam waist  $w_p = 25 \mu\text{m}$  and detection modes of radius  $w_{s,i} = 33 \mu\text{m}$ .

Fig. 1 (a) presents OAM distribution of a biphoton state, which has been prepared by superposing two LG beams with OAM numbers 1 and 5. These modes present a part of the full emission, where the summation in Eq. (2) has been limited to the subspace  $\ell_s, \ell_i = \{-3, -2, \dots, 2, 3\}$  and  $p_s = p_i = 0$ . If we consider only the four modes presented with blue-colored bars on top, we could speak about the four-dimensional entangled state  $|\Psi_4\rangle = \frac{1}{2}(|0, 1\rangle + |1, 0\rangle + |2, 3\rangle + |3, 2\rangle)$  with associated notation  $|p_s = 0, \ell_s, \omega_s\rangle |p_i = 0, \ell_i, \omega_i\rangle := |\ell_s(\omega_s), \ell_i(\omega_i)\rangle$ . Similarly, in Ref. [34], the four-dimensional state  $|\Psi'_4\rangle = \frac{1}{2}(|0, 0\rangle + |1, 1\rangle + |2, 2\rangle + |3, 3\rangle)$  has been generated, but by superposing four LG beams. We will compare these two states in terms of Schmidt number and purity of the spatial state in the subspace  $\ell_s, \ell_i = \{0, 1, 2, 3\}$  and  $p_s = p_i = 0$ , which we refer as  $S_4$ .

In general, a four-dimensional state is maximally entangled if it is pure and possesses a Schmidt number 4. Let us start with the discussion of purity. For the calculation of spatial purity, we need the reduced density matrix  $\rho_{q,s}$ , which results from tracing over the frequency  $\rho_{q,s} = \text{Tr}_\Omega(\rho_s)$  (for more detail see supplementary). Here,  $\rho_s$  stands for the density matrix, and the subscript  $s$  indicates the consideration of the subspace  $S_4$ .

In fact, the calculations show that both states are spatially pure,  $\text{Tr}(\rho_{q,s}^2) = 1$ . The reason is very trivial: all modes that contribute to the states  $|\Psi_4\rangle$  or  $|\Psi'_4\rangle$  consist of only positive OAM numbers, which leads to the same  $N_R = |\ell| - |\ell_s| - |\ell_i| = 0$  for all modes due to  $\ell = \ell_s + \ell_i$ . Moreover, the experimental parameters from [34] satisfies the condition  $z_{R,p} \approx z_{R,i} \approx z_{R,s}$ . Hence, all modes have the same relative Gouy phase and consequently, the same spectrum, which is presented in Fig. 1 (b) with the blue curve. This means that the spatial and spectral DOF are decoupled in  $S_4$ . Interestingly, even though, the authors

did not consider the spectral DOF, the prepared state from Ref. [34] is separable in space and frequency in the subspace, where it lives in. We suppose that the engineering of maximally entangled states in spatial DOF in a certain subspace enforces automatically decoupling in spatial and spectral DOF in that subspace.

The picture is different if we compare the Schmidt numbers of the states  $|\Psi_4\rangle$  and  $|\Psi'_4\rangle$ . The state  $|\Psi_4\rangle$  has Schmidt number 4 and thus is maximally entangled in  $S_4$ . In contrast, the Schmidt number of  $|\Psi'_4\rangle$  equals 2.04, which is smaller than 4 due to non-diagonal modes  $\{|0, 2\rangle, |2, 0\rangle, |1, 3\rangle, |3, 1\rangle\}$  generated in  $S_4$  (see supplementary for comparison). Therefore, the preparation of the state  $|\Psi_4\rangle$  is more efficient in  $S_4$ .

Obviously,  $|\Psi_4\rangle$  is a part of the biphoton state (2) and the full SPDC emission contains further modes. The first four OAM modes out of the subspace  $S_4$  (yellow and orange bars) possess different spectra, shown in Fig. 1 (b) with yellow and orange curves. The appearance of modes with distinguishable spectra increases the spatio-temporal coupling, which, in turn, leads to reduced purity for the spatial biphoton state. In experiments, narrowband filters are usually used in front of detectors to increase the purity of the spatial state. On one hand, the spectral filters improve the purity of the spatial state, on the other hand, they reduce the rate of entangled photons.

In order to quantify the influence of spectral filters on the biphoton state, we calculated the purity of the reduced density matrix depending on the filter bandwidth, but this time for the full emission. As we can see from Fig. 1 (c), very narrow filters are required to end up with a more or less pure state. For instance, a filter with a bandwidth of 1 nm would leave the state in a mixed state of purity 0.33.

The Schmidt number is also different for the full spatio-temporal biphoton state in comparison to the subspace state. The fact of continuous-wave laser leads to the generation of an infinite amount of spectral modes. The only limitation is then the resolution of the detection device. Therefore, we consider only photons with 10 nm range around the central frequency  $810 \pm 10 \text{ nm}$ , which is enough to observe all significant modes in type-II phase-matching configuration [37]. Note that the restriction in the frequency space is equivalent to the restriction in the momentum space, where the optical aperture sets automatically a limit on measurable momentum.

The total Schmidt number of the spatio-temporal biphoton state is calculated from the reduced density matrix in space and frequency for the signal by tracing over the idler  $\rho_{\text{signal}} = \text{Tr}_{\text{idler}}(\rho)$  [16], with Schmidt number being  $K = 1/\text{Tr}(\rho_{\text{signal}}^2)$  [38]. The number of Schmidt modes in the range of frequencies  $810 \pm 10 \text{ nm}$  equals 140. This number refers to both spatial and spectral modes generated in that range. However, this number is not fixed, and it increases with the width of the frequency bandwidth, while the use of a pulsed laser would set an upper limit on the Schmidt number.

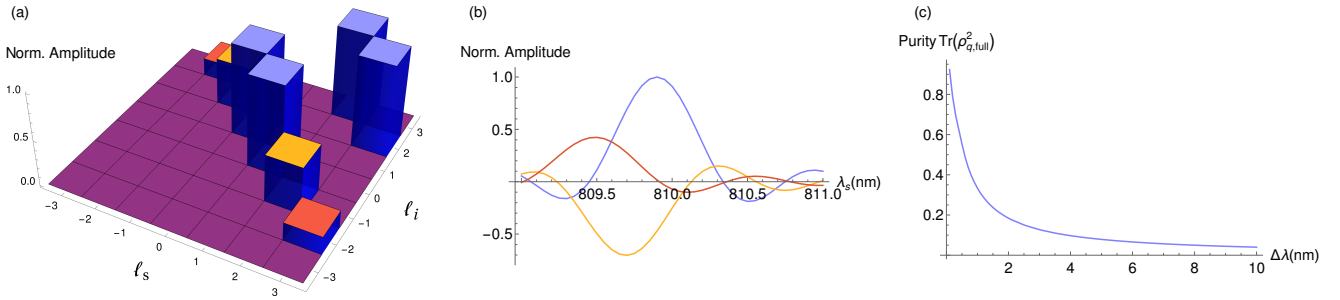


FIG. 1. Normalized high-dimensional entangled state  $\frac{1}{2}(|0,1\rangle + |1,0\rangle + |2,3\rangle + |3,2\rangle)$  (right) and the corresponding spectra (middle). This state is maximally entangled in the subspace  $\ell_s, \ell_i = 0, 1, 2, 3$ . However, side modes are naturally generated out of the subspace. As expected, the modes of signal (idler) involved in the state have the same spectrum (blue curve) compared to the modes out of the subspace shown in the same color as corresponding bars. The left plot corresponds to the purity of the spatial biphoton state depending on the bandwidth of the spectral filter.

The Schmidt number is much smaller in the narrow-band regime, where single spectral modes are assumed. For instance, if we assume that the signal and idler photons are generated only at central frequency  $810\text{ nm}$ , the Schmidt number reduces to 5.8. This indicates that the huge amount of entanglement stored in frequency DOF has been discarded.

We can get rid of the spatio-temporal coupling also in the thin-crystal regime  $L \ll z_{R,p}$ , which assumes that the biphoton state is independent of the crystal features. The problem with this regime is that it gives rise to a huge amount of spatial modes. To illustrate this, we keep all parameters the same as for the state from Fig. 1, except the crystal length  $L = 1\text{ }\mu\text{m}$ . Under this condition, the thin crystal regime is well achieved according to Ref. [13]. The state becomes spatially pure, but possesses a large amount of Schmidt modes,  $10^7$ . Therefore, it is difficult to use calculations done in this regime in a real experiment.

In summary, we derived a closed analytical expression for the biphoton spatio-temporal state in terms of the LG mode amplitudes. The expression readily reveals the dependence of the modal decomposition on frequency and thus correctly describes spectral-spatial coupling, a quintessential feature of SPDC. The expression provides a new understanding of how the Gouy phase is related to the decoupling of spatial and spectral DOF: the relative Gouy phase of the interacting beams fully defines the shape of the spectrum of down-converted photons.

Engineering the modal decomposition of the pump beam can be used to engineer a high-dimensional OAM entanglement. State engineering can also be used to decrease the coupling between the spatial and spectral DOF leading to an increase of the entanglement stored in the spatial DOF. We thus hope that it will aid experimenters in the design and quantitative modeling of challenging experiments based on parametric down-conversion.

The authors thank Egor Kovlakov and Darvin Wanisch for very helpful discussions.

---

[1] A. Anwar, C. Perumangatt, F. Steinlechner, T. Jennewein, and A. Ling, *Review of Scientific Instruments* **92**, 041101 (2021).

[2] H.-S. Zhong, H. Wang, Y.-H. Deng, M.-C. Chen, L.-C. Peng, Y.-H. Luo, J. Qin, D. Wu, X. Ding, Y. Hu, P. Hu, X.-Y. Yang, W.-J. Zhang, H. Li, Y. Li, X. Jiang, L. Gan, G. Yang, L. You, Z. Wang, L. Li, N.-L. Liu, C.-Y. Lu, and J.-W. Pan, *Science* **370**, 1460 (2020).

[3] W. P. Grice, R. S. Bennink, D. S. Goodman, and A. T. Ryan, *Phys. Rev. A* **83**, 023810 (2011).

[4] V. Srivastav, N. H. Valencia, S. Leedumrongwatthanakun, W. McCutcheon, and M. Malik, “Characterising and tailoring spatial correlations in multi-mode parametric downconversion,” (2021), arXiv:2110.03462 [quant-ph].

[5] M. Krenn, M. Huber, R. Fickler, R. Lapkiewicz, S. Ramelow, and A. Zeilinger, *Proceedings of the National Academy of Sciences* **111**, 6243 (2014).

[6] B. Baghdasaryan and S. Fritzsche, *Phys. Rev. A* **102**, 052412 (2020).

[7] Y. Chen, W. Zhang, D. Zhang, X. Qiu, and L. Chen, *Phys. Rev. Applied* **14**, 054069 (2020).

[8] L. Caspani, C. Xiong, B. J. Eggleton, D. Bajoni, M. Liscidini, M. Galli, R. Morandotti, and D. J. Moss, *Light: Science & Applications* **6**, e17100 (2017).

[9] F. Graffitti, P. Barrow, M. Proietti, D. Kundys, and A. Fedrizzi, *Optica* **5**, 514 (2018).

[10] K.-H. Luo, V. Ansari, M. Massaro, M. Santandrea, C. Eigner, R. Ricken, H. Herrmann, and C. Silberhorn, *Opt. Express* **28**, 3215 (2020).

[11] F. M. Miatto, A. M. Yao, and S. M. Barnett, *Phys. Rev. A* **83**, 033816 (2011).

[12] A. M. Yao, *New Journal of Physics* **13**, 053048 (2011).

[13] B. Baghdasaryan, F. Steinlechner, and S. Fritzsche, *Phys. Rev. A* **103**, 063508 (2021).

[14] A. Valencia, A. Ceré, X. Shi, G. Molina-Terriza, and

J. P. Torres, *Phys. Rev. Lett.* **99**, 243601 (2007).

[15] A. Gatti, E. Brambilla, L. Caspani, O. Jedrkiewicz, and L. A. Lugiato, *Phys. Rev. Lett.* **102**, 223601 (2009).

[16] C. I. Osorio, A. Valencia, and J. P. Torres, *New Journal of Physics* **10**, 113012 (2008).

[17] A. Gatti, T. Corti, E. Brambilla, and D. B. Horoshko, *Phys. Rev. A* **86**, 053803 (2012).

[18] B. E. A. Saleh, A. F. Abouraddy, A. V. Sergienko, and M. C. Teich, *Phys. Rev. A* **62**, 043816 (2000).

[19] S. Walborn, C. Monken, S. Pádua, and P. Souto Ribeiro, *Physics Reports* **495**, 87 (2010).

[20] S. Karan, S. Aarav, H. Bharadhwaj, L. Taneja, A. De, G. Kulkarni, N. Meher, and A. K. Jha, *Journal of Optics* **22**, 083501 (2020).

[21] D. S. Tasca, R. M. Gomes, F. Toscano, P. H. Souto Ribeiro, and S. P. Walborn, *Phys. Rev. A* **83**, 052325 (2011).

[22] E. Bolduc, N. Bent, E. Santamato, E. Karimi, and R. W. Boyd, *Optics Letters* **38**, 3546 (2013).

[23] A. Eckstein, B. Brecht, and C. Silberhorn, *Opt. Express* **19**, 13770 (2011).

[24] A. Mair, A. Vaziri, G. Weihs, and A. Zeilinger, *Nature* **412**, 313 (2001).

[25] R. Fickler, R. Lapkiewicz, W. N. Plick, M. Krenn, C. Schaeff, S. Ramelow, and A. Zeilinger, *Science* **338**, 640 (2012), <https://www.science.org/doi/pdf/10.1126/science.1227193>.

[26] K. Fradkin, A. Arie, A. Skliar, and G. Rosenman, *Applied Physics Letters* **74**, 914 (1999), <https://doi.org/10.1063/1.123408>.

[27] W. P. Grice and I. A. Walmsley, *Phys. Rev. A* **56**, 1627 (1997).

[28] W. R. Inc., “Gauss hypergeometric function,” .

[29] D. Kawase, Y. Miyamoto, M. Takeda, K. Sasaki, and S. Takeuchi, *Phys. Rev. Lett.* **101**, 050501 (2008).

[30] F. de Brito, I. da Paz, B. Hiller, J. B. Araujo, and M. Sampaio, *Physics Letters A* **386**, 126989 (2021).

[31] R. F. Offer, A. Daffurn, E. Riis, P. F. Griffin, A. S. Arnold, and S. Franke-Arnold, *Phys. Rev. A* **103**, L021502 (2021).

[32] J. P. Torres, Y. Deyanova, L. Torner, and G. Molina-Terriza, *Phys. Rev. A* **67**, 052313 (2003).

[33] N. Bornman, W. Tavares Buono, M. Love-more, and A. Forbes, *Advanced Quantum Technologies* **4**, 2100066 (2021), <https://onlinelibrary.wiley.com/doi/pdf/10.1002/quate.202100066>.

[34] E. V. Kovlakov, S. S. Straupe, and S. P. Kulik, *Phys. Rev. A* **98**, 060301(R) (2018).

[35] S. Liu, Z. Zhou, S. Liu, Y. Li, Y. Li, C. Yang, Z. Xu, Z. Liu, G. Guo, and B. Shi, *Phys. Rev. A* **98**, 062316 (2018).

[36] J. Spall, *IEEE Transactions on Aerospace and Electronic Systems* **34**, 817 (1998).

[37] F. Steinlechner, M. Gilaberte, M. Jofre, T. Scheidl, J. P. Torres, V. Pruneri, and R. Ursin, *J. Opt. Soc. Am. B* **31**, 2068 (2014).

[38] M. A. Nielsen and I. L. Chuang, *Quantum Computation and Quantum Information* (Cambridge University Press, 2000).

# Supplemental Material: Generalized Description of the Spatio-Temporal Biphoton State in Spontaneous Parametric Down-Conversion

Baghdasar Baghdasaryan,<sup>1, 2</sup> Carlos Sevilla,<sup>3</sup> Fabian Steinlechner,<sup>3, 4</sup> and Stephan Fritzsche<sup>1, 2, 4</sup>

<sup>1</sup> Theoretisch-Physikalisches Institut, Friedrich Schiller University Jena, 07743 Jena, Germany

<sup>2</sup> Helmholtz-Institut Jena, 07743 Jena, Germany

<sup>3</sup> Fraunhofer Institute for Applied Optics and Precision Engineering IOF, 07745 Jena, Germany

<sup>4</sup> Abbe Center of Photonics, Friedrich Schiller University Jena, 07745 Jena, Germany

(Dated: August 19, 2022)

In this supplemental material, we present the technical steps that have been applied, in order to derive the expression for the biphoton state decomposed in LG basis. Moreover, we introduce a theoretical approach for high-dimensional state engineering in OAM basis based on the derived expression.

## I. TECHNICAL DETAILS ABOUT THE DERIVATION OF THE BIPHOTON STATE

We presented the biphoton state in the main text in the momentum space by

$$|\Psi\rangle = \iint d\mathbf{q}_s d\mathbf{q}_i d\omega_s d\omega_i \Phi(\mathbf{q}_s, \mathbf{q}_i, \omega_s, \omega_i) \hat{a}_s^\dagger(\mathbf{q}_s, \omega_s) \hat{a}_i^\dagger(\mathbf{q}_i, \omega_i) |vac\rangle$$

and then decomposed it in LG modes  $|p, \ell, \omega\rangle = \int d\mathbf{q} LG_p^\ell(\mathbf{q}) \hat{a}^\dagger(\mathbf{q}, \omega) |vac\rangle$

$$|\Psi\rangle = \iint d\omega_s d\omega_i \sum_{p_s, p_i=0}^{\infty} \sum_{\ell_s, \ell_i=-\infty}^{\infty} C_{p_s, p_i}^{\ell_s, \ell_i} |p_s, \ell_s, \omega_s\rangle |p_i, \ell_i, \omega_i\rangle, \quad (S1)$$

where the coincidence amplitudes are calculated from the overlap integral  $C_{p_s, p_i}^{\ell_s, \ell_i} = \langle p_s, \ell_s, \omega_s; p_i, \ell_i, \omega_i | \Psi \rangle$ ,

$$C_{p_s, p_i}^{\ell_s, \ell_i} = \iint d\mathbf{q}_s d\mathbf{q}_i \Phi(\mathbf{q}_s, \mathbf{q}_i, \Omega_s, \Omega_i) [LG_{p_s}^{\ell_s}(\mathbf{q}_s)]^* \times [LG_{p_i}^{\ell_i}(\mathbf{q}_i)]^*. \quad (S2)$$

The angular distribution of a LG mode with quantum numbers  $p$  and  $\ell$  in the momentum space is given by

$$LG_p^\ell(\rho, \varphi) = e^{-\frac{\rho^2 w^2}{4}} e^{i\ell\varphi} \sum_{u=0}^p T_u^{p, \ell} \rho^{2k+|\ell|} \quad (S3)$$

with  $T_u^{p, \ell}$  being

$$T_u^{p, \ell} = \sqrt{\frac{p!(p+|\ell|)!}{\pi}} \left(\frac{w}{\sqrt{2}}\right)^{2u+|\ell|+1} \frac{(-1)^{p+u}(i)^\ell}{(p-u)!(|\ell|+u)!u!},$$

and where  $\rho$  and  $\varphi$  stand for the cylindrical coordinates  $\mathbf{q} = (\rho, \varphi)$ .

The biphoton mode function reads as

$$\Phi(\mathbf{q}_s, \mathbf{q}_i, \omega_s, \omega_i) = N_0 LG_p^\ell(\mathbf{q}_s + \mathbf{q}_i) e^{-(\omega_s + \omega_i)^2 t_0^2/4} \frac{t_0}{\sqrt{\pi}} \times \int_{-L/2}^{L/2} dz \exp[i\Delta k^z z], \quad (S4)$$

where we modeled the angular distribution of the pump with a LG beam and the temporal distribution with a Gaussian envelope of a pulse duration  $t_0$ . We used the cylindrical coordinates to present the phase mismatch in the z-direction  $\Delta k^z$  as

$$\Delta k^z = \Delta_\Omega + \rho_s^2 \frac{k_p - k_s}{2k_p k_s} + \rho_i^2 \frac{k_p - k_i}{2k_p k_i} - \frac{\rho_s \rho_i}{k_p} \cos(\varphi_i - \varphi_s), \quad (S5)$$

where the frequency part  $\Delta_\Omega$  is given by

$$\Delta_\Omega = \frac{\Omega_s + \Omega_i}{u_p} - \frac{\Omega_s}{u_s} - \frac{\Omega_i}{u_i} + \frac{G_p(\Omega_s + \Omega_i)^2}{2} - \frac{G_s \Omega_s^2}{2} - \frac{G_i \Omega_i^2}{2}. \quad (S6)$$

We can now substitute Eqs. (S3)-(S6) into Eq. (S2), in order to calculate the coincidence amplitudes:

---


$$C_{p_s, p_i}^{\ell_s, \ell_i} = N_0 \sum_{u=0}^p \sum_{i=0}^{p_s} \sum_{j=0}^{p_i} T_u^{p, \ell} (T_i^{p_s, \ell_s})^* (T_j^{p_i, \ell_i})^* \int dz d\rho_s d\rho_i d\varphi_s d\varphi_i \Theta(z, \rho_s, \rho_i, \varphi_i - \varphi_s) e^{i\ell\varphi_s} e^{i(-\ell_s\varphi_s - \ell_i\varphi_i)}, \quad (S7)$$

Where we defined the function  $\Theta(z, \rho_s, \rho_i, \varphi_i - \varphi_s)$  as

$$\begin{aligned} \Theta(z, \rho_s, \rho_i, \varphi_i - \varphi_s) = & [\rho_s^2 + \rho_i^2 + 2\rho_s\rho_i \cos(\varphi_i - \varphi_s)]^{\frac{2u+|\ell|-|\ell|}{2}} \rho_s^{|\ell_s|+2i+1} \rho_i^{|\ell_i|+2j+1} (\rho_s + \rho_i e^{i(\varphi_i - \varphi_s)})^{\ell} \\ & \times \exp \left[ -\frac{[\rho_s^2 + \rho_i^2 + 2\rho_s\rho_i \cos(\varphi_i - \varphi_s)] w^2}{4} - \frac{\rho_s^2 w_s^2}{4} - \frac{\rho_i^2 w_i^2}{4} \right] \frac{t_0}{\sqrt{\pi}} e^{-\frac{t_0^2(\Omega_s + \Omega_i)^2}{4}} \\ & \times \exp \left[ iz \left( \Delta_\Omega + \rho_s^2 \frac{k_p - k_s}{2k_p k_s} + \rho_i^2 \frac{k_p - k_i}{2k_p k_i} - \cos(\varphi_i - \varphi_s) \frac{\rho_s \rho_i}{k_p} \right) \right]. \end{aligned} \quad (\text{S8})$$

The polar angle  $\varphi$  of the pump beam (see Eq. (S3)) has been expressed as function of signal and idler coordinates

$$e^{i\ell\varphi} = [\cos(\varphi) + i \sin(\varphi)]^\ell = \frac{e^{i\ell\varphi_s}}{\rho^\ell} [\rho_s + \rho_i e^{i(\varphi_i - \varphi_s)}]^\ell,$$

by taking into account the conservation of transverse momentum

$$\mathbf{q}_p = \mathbf{q}_s + \mathbf{q}_i = \begin{pmatrix} \rho_s \cos \varphi_s + \rho_i \cos \varphi_i \\ \rho_s \sin \varphi_s + \rho_i \sin \varphi_i \end{pmatrix}.$$

The presentation of coincidence amplitudes  $C_{p_s, p_i}^{\ell_s, \ell_i}$  in Eq. (S7) with the function  $\Theta(\rho_s, \rho_i, \varphi_i - \varphi_s)$  follows the goal to show the OAM-conservation in SDPC. To do so, we expand the function  $\Theta(\rho_s, \rho_i, \varphi_i - \varphi_s)$  as superposition of plane waves with the phases  $\exp[i\ell'(\varphi_i - \varphi_s)]$  (Fourier series with complex coefficients)

$$\Theta(z, \rho_s, \rho_i, \varphi_i - \varphi_s) = \sum_{\ell'=-\infty}^{\infty} f_{\ell'}(z, \rho_s, \rho_i) e^{i\ell'(\varphi_i - \varphi_s)}. \quad (\text{S9})$$

We substitute the expression (S9) into Eq. (S7) and perform the integration over the polar angles  $\varphi_s$  and  $\varphi_i$ :

$$\begin{aligned} & \sum_{\ell'=-\infty}^{\infty} f_{\ell'}(z, \rho_s, \rho_i) \int_0^{2\pi} \int_0^{2\pi} e^{i\ell\varphi_s} e^{i(-\ell_s \varphi_s - \ell_i \varphi_i)} \\ & \times e^{i\ell'(\varphi_i - \varphi_s)} d\varphi_s d\varphi_i \propto \delta_{\ell', \ell - \ell_s} \delta_{\ell', \ell_i}. \end{aligned} \quad (\text{S10})$$

As expected, the Kronecker delta functions appear in Eq. (S10) that enforce the conservation of OAM  $\ell - \ell_s = \ell_i$ . This conservation is not valid out of the quasi-collinear regime [1] because of the spin-orbital angular momentum coupling in non-paraxial regime [2]. In a non-collinear regime, the total angular momentum should remain conserved, which can be a future topic to study.

Going back to the expression (S7), we now calculate the integration over polar coordinates  $\varphi_{s,i}$  explicitly. For simplicity, we consider the coincidence amplitudes  $C_{p_s, p_i}^{\ell_s, \ell_i}$  (revised notation to consider the mode numbers of the pump mode) for positive OAM number of pump beam  $\ell \geq 0$ . The coincidence amplitude for  $\ell < 0$  are then given by  $C_{p_s, p_i}^{\ell_s, \ell_i} = (C_{p_s, p_i}^{-\ell_s, -\ell_i})^*$ , which follows from Eq. (S2). Furthermore, the two brackets on the first line in Eq. (S8) should be rewritten as finite sums by using the Binomial formula. For instance, the first

bracket is written as

$$\begin{aligned} [\rho_s^2 + \rho_i^2 + 2\rho_s\rho_i \cos(\varphi_i - \varphi_s)]^u = & \sum_{m=0}^u \binom{u}{m} (\rho_s^2 + \rho_i^2)^{u-m} \\ & \times [2\rho_s\rho_i \cos(\varphi_i - \varphi_s)]^m. \end{aligned}$$

The *cosine* function can be expressed as the sum of two exponential functions by using the Euler's formula, which should then be again expressed as a Binomial sum. After this step, the angular integration takes the form of the integral representation of Bessel function of the first kind [3]

$$\frac{1}{2\pi} \int_0^{2\pi} e^{in\varphi \pm iz \cos(\varphi - \varphi')} d\varphi = (\pm i)^n e^{in\varphi'} J_n(z).$$

Next, the sum representation of the Bessel function should be used

$$J_n(z) = \sum_{k=0}^{\infty} \frac{(-1)^k}{k! \Gamma(k+n+1)} \left( \frac{z}{2} \right)^{2k+n}, \quad (\text{S11})$$

which transforms the integration over the radial coordinates into

$$\int_0^{\infty} d\rho \rho^n e^{-a\rho^2} = \frac{\Gamma(\frac{n+1}{2})}{2a^{\frac{n+1}{2}}}.$$

The final result is achieved via summing over  $k$  from Eq. (S11) by using the definition of the *Regularized* hypergeometric function [4]

$$\begin{aligned} C_{p_s, p_i}^{\ell_s, \ell_i} = & N_0 \pi^{3/2} t_0 e^{-\frac{t_0^2(\Omega_s + \Omega_i)^2}{4}} \delta_{\ell, \ell_s + \ell_i} \\ & \sum_{u=0}^p \sum_{s=0}^{p_s} \sum_{i=0}^{p_i} T_u^{p, \ell} (T_s^{p_s, \ell_s})^* (T_i^{p_i, \ell_i})^* \sum_{n=0}^{\ell} \sum_{m=0}^u \\ & \binom{\ell}{n} \binom{u}{m} \sum_{f=0}^{u-m} \sum_{v=0}^m \binom{u-m}{f} \binom{m}{v} \Gamma[h] \Gamma[b] \\ & \int_{-L/2}^{L/2} dz e^{iz\Delta_\Omega} \frac{D^d}{H^h B^b} {}_2F_1 \left[ h, b, 1+d, \frac{D^2}{H B} \right] \end{aligned} \quad (\text{S12})$$

where the coefficients are given by

$$\begin{aligned} H &= \frac{w_p^2}{4} + \frac{w_s^2}{4} - iz \frac{k_p - k_s}{2k_p k_s}, & D &= -\frac{w_p^2}{4} - iz \frac{1}{2k_p}, \\ B &= \frac{w_p^2}{4} + \frac{w_i^2}{4} - iz \frac{k_p - k_i}{2k_p k_i}, & d &= \ell_i + m - n - 2v, \\ h &= \frac{1}{2}(2 + 2s + \ell + \ell_i + 2(-f + u) - 2n - 2v + |\ell_s|), \\ b &= \frac{1}{2}(2 + 2f + 2i + \ell_i + 2m - 2v + |\ell_i|). \end{aligned}$$

Note that the narrowband regime is achieved via dropping out the terms  $e^{iz\Delta_\Omega}$  and the temporal distribution of the pump in Eq. (S12) and the perfect thin-crystal regime, by letting the length of the crystal tend to zero  $L \rightarrow 0$ , which mathematically means to integrate over the delta function  $\delta(z = 0)$ .

## II. ENGINEERING HIGH-DIMENSIONAL ENTANGLED STATES IN OAM BASIS

Here, we show, how to engineer high-dimensional entangled states in LG basis via using the expression (S12). For illustration, let us consider entangled states generated experimentally in OAM basis by Kovlakov *et al.* by superposing different LG beams [5]. The necessary pump has been calculated with the simultaneous perturbation stochastic approximation (SPSA) algorithm. Below, we will construct the same state in a more straightforward way, without using any optimization algorithm.

It is enough for our purpose to construct a single state from Ref. [5]. We consider the subspace  $\ell_s, \ell_i = 0, 1, 2, 3$  and  $p_s = p_i = 0$ , which we refer as  $S_4$ , with associated notation  $|p_s = 0, \ell_s, \omega_s\rangle |p_i = 0, \ell_i, \omega_i\rangle := |\ell_s(\omega_s), \ell_i(\omega_i)\rangle$ , where the four-dimensional state  $|\Psi'_4\rangle = \frac{1}{2}(|0, 0\rangle + |1, 1\rangle + |2, 2\rangle + |3, 3\rangle)$  has been engineered. We can enhance the preparation of such kind of state, if the subspace, where it is maximally entangled, is larger. In general, for a given maximal values of  $\ell_s$  and  $\ell_i$ , the pump beam should be at least superposition of LG beams with the range of OAM  $\ell = [\min(\ell_s + \ell_i), \max(\ell_s + \ell_i)]$ . Therefore, the pump for the subspace  $S_4$  is modeled as following:

$$V_p = \sum_{\ell=0}^6 a_\ell \text{LG}_0^\ell,$$

where the expansion amplitudes  $a_\ell$  should still be determined. The corresponding state is constructed by using Eq. (S1)

$$|\Psi_4\rangle = \sum_{\ell=0}^6 a_\ell \sum_{\ell_s, \ell_i=0}^3 C_{0,0,0}^{\ell, \ell_s, \ell_i} |\ell_s, \ell_i\rangle.$$

The task is now to choose appropriate values for  $a_\ell$ , in order to generate the desired high-dimensional state. The

matrix representation of the state  $|\Psi_4\rangle$  is given by the left-hand side of the following expression

$$\begin{pmatrix} a_0 C_{0,0} & a_1 C_{1,0} & a_2 C_{2,0} & a_3 C_{3,0} \\ a_1 C_{0,1} & a_2 C_{1,1} & a_3 C_{2,1} & a_4 C_{3,1} \\ a_2 C_{0,2} & a_3 C_{1,2} & a_4 C_{2,2} & a_5 C_{3,2} \\ a_3 C_{0,3} & a_4 C_{1,3} & a_5 C_{2,3} & a_6 C_{3,3} \end{pmatrix} \rightarrow \begin{pmatrix} 0 & 1 & 0 & 0 \\ 1 & 0 & 0 & 0 \\ 0 & 0 & 0 & 1 \\ 0 & 0 & 1 & 0 \end{pmatrix}, \quad (\text{S13})$$

where we used the notation  $C_{0,0,0}^{\ell_s + \ell_i, \ell_s, \ell_i} = C_{\ell_s, \ell_i}$ . Maximally entangled state in this subspace means to have four linear independent columns (rows). The right-hand side of the expression (S13) is such a state that can be engineered if we select  $a_1 = 1/C_{0,1} \approx 1/C_{1,0}$ ,  $a_5 = 1/C_{2,3} \approx 1/C_{3,2}$  and  $a_0 = a_2 = a_3 = a_4 = a_6 = 0$ . This choice leads to the maximally entangled state  $|\Psi_4\rangle = \frac{1}{2}(|0, 1\rangle + |1, 0\rangle + |2, 3\rangle + |3, 2\rangle)$ . Thus, the state engineering is finished, where the coefficients of the pump superposition  $\{a_1, a_5\}$  should be calculated with the expression (S12) based on experimental parameters (see Fig. 1 (a)).

The state  $|\Psi'_4\rangle = \frac{1}{2}(|0, 0\rangle + |1, 1\rangle + |2, 2\rangle + |3, 3\rangle)$  from Ref. [5] can also be engineered, if we select  $\{a_0, a_2, a_4, a_6\}$

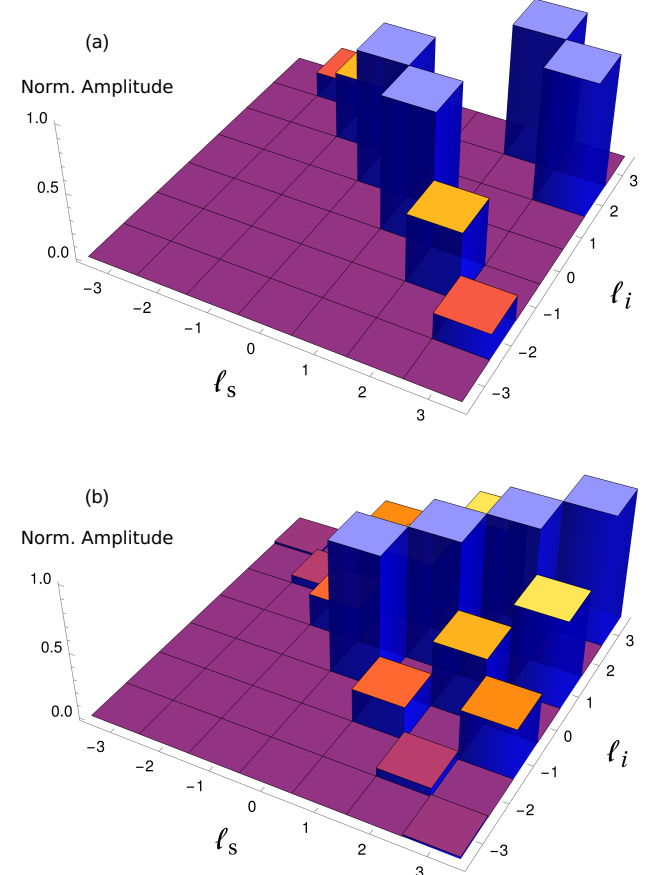


FIG. 1. High dimensional entangled state  $\frac{1}{2}(|0, 1\rangle + |1, 0\rangle + |2, 3\rangle + |3, 2\rangle)$  (a), and high dimensional entangled state  $\frac{1}{2}(|0, 0\rangle + |1, 1\rangle + |2, 2\rangle + |3, 3\rangle)$  (b).

to be equal to  $\{1/C_{0,0}, 1/C_{1,1}, 1/C_{2,2}, 1/C_{3,3}\}$  and  $a_1 = a_3 = a_5 = 0$ . However, this choice leads to generation of non-desirable diagonal modes  $\{C_{0,2}, C_{2,0}, C_{1,3}, C_{3,1}\}$  (see Fig. 1 (b)), which leads to decrease of entanglement.

### III. PURITY OF SPATIAL BIPHOTON STATE

In order to calculate the spatial purity of the biphoton state, we need the reduced density matrix  $\rho_{\mathbf{q}}$ , which results from tracing over the frequency  $\rho_{\mathbf{q}} = \text{Tr}_{\Omega}(\rho)$ . For a continuous wave laser, the deviations of signal and idler photons energies from the central frequencies have opposite signs  $\Omega_s = -\Omega_i := \Omega$ . Here, we again consider for simplicity  $p_s = p_i = 0$ . With this in mind, Eq. (S1) transforms into

$$|\Psi\rangle = \iint d\Omega \sum_{\ell_s, \ell_i=-\infty}^{\infty} C_{\ell_s, \ell_i}(\Omega) |\ell_s, \Omega\rangle |\ell_i, -\Omega\rangle \quad (\text{S14})$$

Now, we calculate the density matrix  $\rho = |\Psi\rangle\langle\Psi|$  and then we trace over the spectral domain, which yields:

$$\rho_{\mathbf{q}} = \sum_{\ell_s, \ell_i} \sum_{\tilde{\ell}_s, \tilde{\ell}_i} A_{\ell_s, \ell_i}^{\tilde{\ell}_s, \tilde{\ell}_i} |\ell_s, \ell_i\rangle \langle \tilde{\ell}_s, \tilde{\ell}_i| \quad (\text{S15})$$

where  $A_{\ell_s, \ell_i}^{\tilde{\ell}_s, \tilde{\ell}_i} = \int d\Omega C_{\ell_s, \ell_i}(\Omega) [C_{\tilde{\ell}_s, \tilde{\ell}_i}(\Omega)]^*$  is the overlap integral of the spectra of the OAM modes. Eq. (S15) is very useful to calculate the spatial purity in small subspaces. For instance, we can run summations in Eq. (S15) over  $\ell_s, \ell_i, \tilde{\ell}_s, \tilde{\ell}_i = 0, 1, 2, 3$ , renormalize the state, contract the density matrix of the subspace  $\rho_{\mathbf{q}, s}$  and calculate the purity  $\text{Tr}(\rho_{\mathbf{q}, s}^2)$ . The purity of the both states  $|\Psi'_4\rangle$  and  $|\Psi_4\rangle$  equals to one, since all modes contributing to these states have the same spectrum.

### REFERENCES

- [1] G. Molina-Terriza, J. P. Torres, and L. Torner, *Optics Communications* **228**, 155 (2003).
- [2] B. Bagdasaryan, B. Böning, W. Paufler, and S. Fritzsche, *Phys. Rev. A* **99**, 023403 (2019).
- [3] H. A. Yousif and R. Melka, *Computer Physics Communications* **106**, 199 (1997).
- [4] W. R. Inc., “Gauss hypergeometric function,” .
- [5] E. V. Kovlakov, S. S. Straupe, and S. P. Kulik, *Phys. Rev. A* **98**, 060301 (2018).